Interactions between actin and myosin filaments in skeletal muscle visualized in frozen-hydrated thin sections

B. L. Trus,* A. C. Steven,‡ A. W. McDowall,‖ M. Unser,§ J. Dubochet,‖ and R. J. Podolsky‡

*Computer Systems Laboratory, Division of Computer Research and Technology, ‡Laboratory of Physical Biology, National Institute of Arthritis, Musculoskeletal and Skin Diseases,§ Biological Engineering and Instrumentation Branch, National Institutes of Health, Bethesda, Maryland 20892; and ‖European Molecular Biology Laboratory, D-6900 Heidelberg, Federal Republic of Germany

ABSTRACT For the purpose of determining net interactions between actin and myosin filaments in muscle cells, perhaps the single most informative view of the myofilament lattice is its averaged axial projection. We have studied frozen-hydrated transverse thin sections with the goal of obtaining axial projections that are not subject to the limitations of conventional thin sectioning (suspect preservation of native structure) or of equatorial x-ray diffraction analysis (lack of experimental phases). In principle, good preservation of native structure may be achieved with fast freezing, followed by low-dose electron imaging of unstained vitrified cryosections. In practice, however, cryosections undergo large-scale distortions, including irreversible compression; furthermore, phase contrast imaging results in a nonlinear relationship between the projected density of the specimen and the optical density of the micrograph.

To overcome these limitations, we have devised methods of image restoration and generalized correlation averaging, and applied them to cryosections of rabbit psoas fibers in both the relaxed and rigor states. Thus visualized, myosin filaments appear thicker than actin filaments by a much smaller margin than in conventional thin sections, and particularly so for rigor muscle. This may result from a significant fraction of the myosin S1-cross-bridges averaging out in projection and thus contributing only to the baseline of projected density. Entering rigor incurs a loss of density from an annulus around the myosin filament, with a compensating accumulation of density around the actin filament. This redistribution of mass represents attachment of the fraction of cross-bridges that are visible above background. Myosin filaments in the "nonoverlap" zone appear to broaden on entering rigor, suggesting that, on deprivation of ATP, cross-bridges in situ move outwards even without actin in their immediate proximity.

INTRODUCTION

According to the "sliding filament" theory (1–3), muscles contract and force is generated by a molecular mechanism whereby two interdigitating systems of inextensible protein filaments slide past each other into a condition of greater overlap. Each contractile unit (sarcomere) contains an aligned bundle of "thick" myosin filaments, with the "thin" actin filaments inserted between them. Laterally, the myosin filaments are packed in a hexagonal array, with the actin filaments positioned (in the case of vertebrate skeletal muscle) at the trigonal points of this myosin-based lattice. It is, by now, widely accepted that force generation is mediated by "cross-bridges" that protrude from the backbones of the myosin filaments and couple transiently with adjacent actin filaments. However, many details remain obscure (4). For instance, the numbers of distinct conformational states that may be assumed by cross-bridges, as well as the fractional occupancies of these states, have still to be pinned down for both relaxed and activated muscles.

For the purpose of inferring net interfilament interactions in the myofilament lattice, perhaps the most revealing single view of this complex three-dimensional matrix is its axial projection. Two experimental approaches, equatorial x-ray fiber diffraction analysis (e.g. references 5–10) and electron microscopy of transverse thin sections (e.g. references 6, 11, 12), have been extensively used to obtain representations of this view. Both have characteristic advantages and limitations. With x-ray diffraction, the map of projected density is obtained by Fourier synthesis, combining experimental amplitudes with phases that are assigned indirectly, usually by modeling. Such maps have the advantage that the x-ray data are obtained from native muscle; on the other hand, their phases are not experimentally determined quantities, and the values of the amplitudes extracted from equatorial intensity traces depend, to some extent, on assumptions about the background subtraction. Moreover, the resulting map is a total axial average that coprojects regions of the A band where the myosin and actin filaments overlap with regions where they do not. In electron micrographs of transverse thin sections, the issue of phase ambiguity does not arise, and different axial levels within the sarcomere may be sam-

A. W. McDowall's present address is Howard Hughes Medical Institute, 5323 Harry Hynes Blvd., Dallas, TX 75325.

J. Dubochet's present address is Centre de Microscopie Electronique, 27 Rue du Bugnon, CH-1005 Lausanne, Switzerland.

pled and compared. On the other hand, interpretation of such images is clouded by reservations as to how well native structure is preserved by chemical fixation, and how uniformly the myofilament proteins respond to positive staining.

Electron microscopy of unstained thin sections of muscles preserved in vitreous ice by rapid freezing (13–16) has the potential to combine the advantages of both of the above methods, in the sense of providing direct visualization of specimens that are maintained in their native states. In practice, however, certain problems arise. Frozen sections are subject to large-scale distortions (buckling, folding) and cutting-induced compression (13, 14), so that only very small areas of genuine transverse section are obtained, and even these are severely disordered. Moreover, their contrast is so low as to require the use of heavily underfocused phase contrast imaging, so that specimen density is not conveyed in a linear manner (15). In an attempt to overcome these difficulties and thus help realize the potential of cryosectioning, we have developed image processing methods intended to compensate for spatial disordering and nonuniformity of contrast transfer. Here we describe this approach and apply it to cryosections of rabbit psoas muscle in both the relaxed and rigor states.

MATERIALS AND METHODS

Preparation of muscle fibers

Single-skinned fibers were prepared from rabbit psoas muscle. Fiber bundles were removed from anesthetized rabbits and immersed in skinning solution (Table 1) for at least 12 h. A fiber bundle was then transferred to a chamber containing relaxing solution at 5°C, with 15% (440 mM) sucrose added as cryoprotectant (Table 1). Single fibers were teased out and draped over the outer surface of a gold-plated mount consisting of two L-shaped pins held in a L-⌟ configuration by a common Bakelite centerpiece. The ends of the fiber were then attached with cellulose to the exposed ends of the pins, without allowing the fiber surface to dry. The mount with attached fiber was transferred to a chilled petri dish, and the fiber covered with several drops of cryoprotectant-containing relaxing or rigor solution (Table 1). In some experiments, creatine phosphokinase (Sigma Chemical Co., St. Louis, MO, 2 mg/ml) was added to the relaxing solution.

TABLE 1 Solution compositions

	Skinning	Relaxing	Rigor
Potassium propionate	150	35	80
Potassium phosphate	5	—	—
Imidazole	—	10	10
Magnesium acetate	3	—	—
Magnesium chloride	—	5	5
EGTA	3	3	3
ATP	3	3	—
Creatine phosphate	—	10	—
Sucrose	—	440	440
Ionic strength	170	100	100

All solutions were adjusted to pH 7.0 at 4°C. Units are millimoles.

Freezing, cryosectioning, and electron microscopy

Freezing was carried out in a cold room (5°C). The fiber mount was attached to a movable piston, and excess solution adhering to the fiber segment was gently blotted off with filter paper. The blotting maneuver was monitored with a dissecting microscope. Rapid freezing was then performed by releasing the piston to drive the fiber mount assembly into liquid ethane cooled close to the solidification temperature. The assembly was then transferred into liquid-N_2, and the fiber broken by separating the two L-shaped pins. One of the pins was clamped into the chuck of the cryoultramicrotome (model FC4, Reichert Scientific Instruments, Buffalo, NY), and sections were cut with a diamond knife at −160°C and stored under liquid N_2 until use. At this point, the sections were transferred into a precooled model 626 cryoholder (Gatan, Inc., Warrendale, PA) as described (13, 16) and observed according to low-dose procedures, at magnifications of 11,700 and 15,200, in a Philips EM400 electron microscope at defocus settings, typically of 3–4 μm.

Image processing

Digitization and general image processing methodology

Those micrographs which showed regions of the myofilament lattice in transverse section were selected for analysis. They were digitized by means of a model 1010MG flatbed scanning microdensitometer (Perkin-Elmer Corp., Norwalk, CT) (17), using a square aperture whose sidelength was equal to the step size of the scanning raster, and corresponded to 1.25 nm at the specimen. The overall analysis followed the plan shown in Fig. 1. Standard image processing operations were performed using the PIC system (18), and the techniques developed specifically for this project and incorporated into PIC are described in greater detail below. These programs were run on a VAX 11/780 in conjunction with a model IP8500 image processor (Gould Inc., Freemont, CA) with color television monitor, and a model 4007 multiformat camera station (Matrix, Instruments Inc., Orangeburg, NY).

Image restoration

The digitized micrographs were first transformed in order to correct as well as possible for the nonuniformity of contrast transfer in different spatial frequency domains that is incurred by strongly underfocused coherent bright-field imaging (19). In broad outline, the background noise component of the Fourier transform of a given image was used to make an empirical construction of its contrast transfer function (20). This function defined a set of weight factors that were used to rescale the terms of the Fourier transform. Finally, the "restored" image was obtained by inverse Fourier transformation.

Specifically, each area of 256 × 256 densities was first corrected for density gradients by fitting a bilinear function,

$$\rho_{BG}(x,y) = a.x + b.y + c.x.y + d,$$

to it, and then subtracting this background. The image was then Fourier-transformed, and its full-plane diffraction pattern (amplitude spectrum) displayed on the monitor. The pattern (e.g., Fig. 4 *b*) contained a set of periodic reflections that were relatively intense

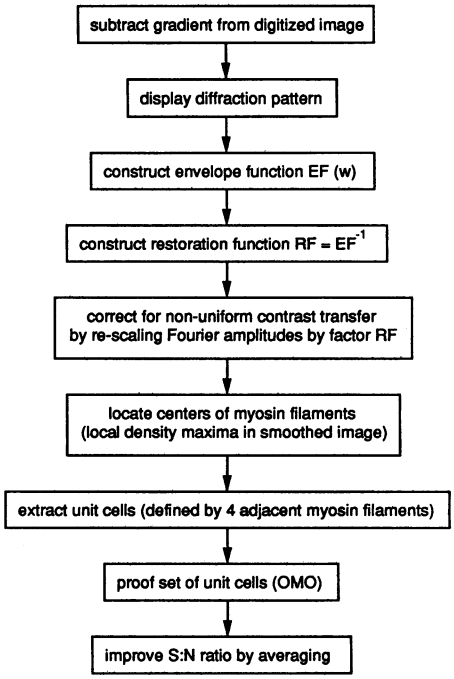

FIGURE 1 Flow chart listing sequence of image processing operations applied to original electron micrograph data in analysis of frozen-hydrated transverse thin sections of muscle fibers.

(although generally diffuse on account of spatial disordering), in a background of spectral "noise". Interactively, the operator masked out the periodic reflections, and the contrast transfer function (CTF) was operationally defined by local averaging of the residual diffraction pattern. Based on the premise that the CTF should be smoothly varying, each pixel was replaced by the local average over a 17 × 17 square centered on it, with masked Fourier orders omitted from the average. (The disorder-related smearing of the reciprocal lattice reflections made it necessary to use such a large averaging window). Finally, this envelope function, EF(w), was symmetrized twofold. From this approximation to the CTF, a "restoration function", RF(w), was defined, whose dependence on spatial frequency (w) was given as follows.

$$\text{When } w < w_0\,,\ \mathrm{RF}(\mathbf{w}) = \mathrm{EF}(\mathbf{w}_0)/\mathrm{EF}(\mathbf{w})\,.$$

Restoration was effected by multiplying the amplitude of each component of the original Fourier transform by the factor RF(w). The threshold, $\mathbf{w}_0$, was routinely taken on 0.2 nm^{-1}, and beyond $\mathbf{w}_0$, no restoration was attempted, i.e., RF(w) = 1 for $w > w_0$.

This approach is based on the supposition that, over the limited spatial frequency range of current interest (i.e., out to ~0.2 nm^{-1}), the background noise is uncorrelated, i.e., it is white noise, at least to a first approximation. Our preference for this parameter-free method, as opposed to using some analytical expression for the CTF with assigned parameters, stems primarily from uncertainty as to an appropriate formalism, because the cryosection images are evidently not pure phase objects (e.g., contrast transfer does not fall to zero at the Fourier space origin). In its favor, the envelope functions constructed by our method do reproduce the major features to be expected of a contrast transfer mechanism that is dominated, but not monopolized, by phase contrast, i.e., they increase smoothly to a maximum (reaching about double their value near the origin), and then fall off monotonically. There was some limited variation from micrograph to micrograph in the spatial frequency of this maximum, and in the ellipticity of the lobe, the latter effect relating to astigmatism and/or drift. Consequently, correction functions had to be tailored individually for each micrograph.

So far, on account of the limited resolution range currently achieved, our image restoration operations have been confined to the primary lobe of the CTF, and we have not had to confront the riskier proposition of spatial frequency domains that contain zeros of the CTF or require contrast reversal (15, 20, 21). The procedure was tested by using it to restore computer-generated model lattices which had been "imaged" with CTFs resembling those encountered in the experimental micrographs.

Correlation averaging

Numerous computational methods have been described for rectifying imperfectly ordered lattices (e.g., reference 22). However the degree of disorder encountered in these cryosections was such as to require a treatment adapted particularly to this purpose. The principle of our method, which incorporates many of the procedures used earlier by Crowther and Sleytr (23), is to locate the centers of myosin filaments and use them as fiducial markers, four adjacent centers defining a unit cell. Local spatial distortions were rectified by mapping each unit cell into a cell of standard dimensions. (We use the rectangular super-cell convention for hexagonal lattices [24] with 30 × 52 pixels). The myosin filament centers were located automatically by a program that compiled a list of the coordinates of the local density maxima in a low-pass filtration of the area under study. This area was then displayed on the monitor, with the maxima identified by colored crosses on a graphics overlay plane. Working interactively with a tablet/mouse system, the operator then picked out the quartets of points that enclosed the unit cells. All potentially useful unit cells (i.e., without obvious defects) were extracted from each area, applying bilinear interpolation to the restored (but not low-pass filtered) representation. Finally, any anomalous unit cells were eliminated by screening the complete data set with the OMO algorithm (25), which operates according to a criterion of mutual consistency. Typically, ~70% of the unit cells were approved by OMO, and these were averaged. Resolution was assessed according to the "spectral signal-to-noise ratio" (SSNR) criterion (26).

The major distortion which the cryosections undergo is cutting-induced compression (13, 14), and the procedure that we have used to compensate for it is based on the assumption that protein and ice are approximately equally compressible. There is, in fact, evidence that folded proteins are quite resistant to compression, having compressibilities that areof the same order, albeit slightly smaller, than those of water and ice (27, 28).

The myofilament lattice constant was measured as the center-to-center distance between myosin filaments, averaging over three to five lattice steps in the direction of least compression (i.e., the longest interfilament spacing). The result, 45.3 ± 3.1 nm (SD, n = 30), is close to the value obtained by x-ray fiber diffraction for rabbit psoas muscle at 100 mM ionic strength and 5°C in the absence of sucrose (10). No significant difference was found for the rigor state. Accordingly, all dimensions given are scaled according to this calibration.

For comparative display of the averaged relaxed and rigor unit cells (e.g., Figs. 7 and 8 and Table 3), the images were normalized so that (*a*) they contained the same total mass, and (*b*) the central 8 nm (diameter) of the myosin filament should also contain the same amount of mass. The latter constraint was adopted, based on the likelihood that little or no net change affects this part of the unit cell in the transition between relaxation and rigor (8). Essentially the same results were obtained using an alternative normalization procedure whereby the images were constrained to have the same mass and dynamic power (energy).

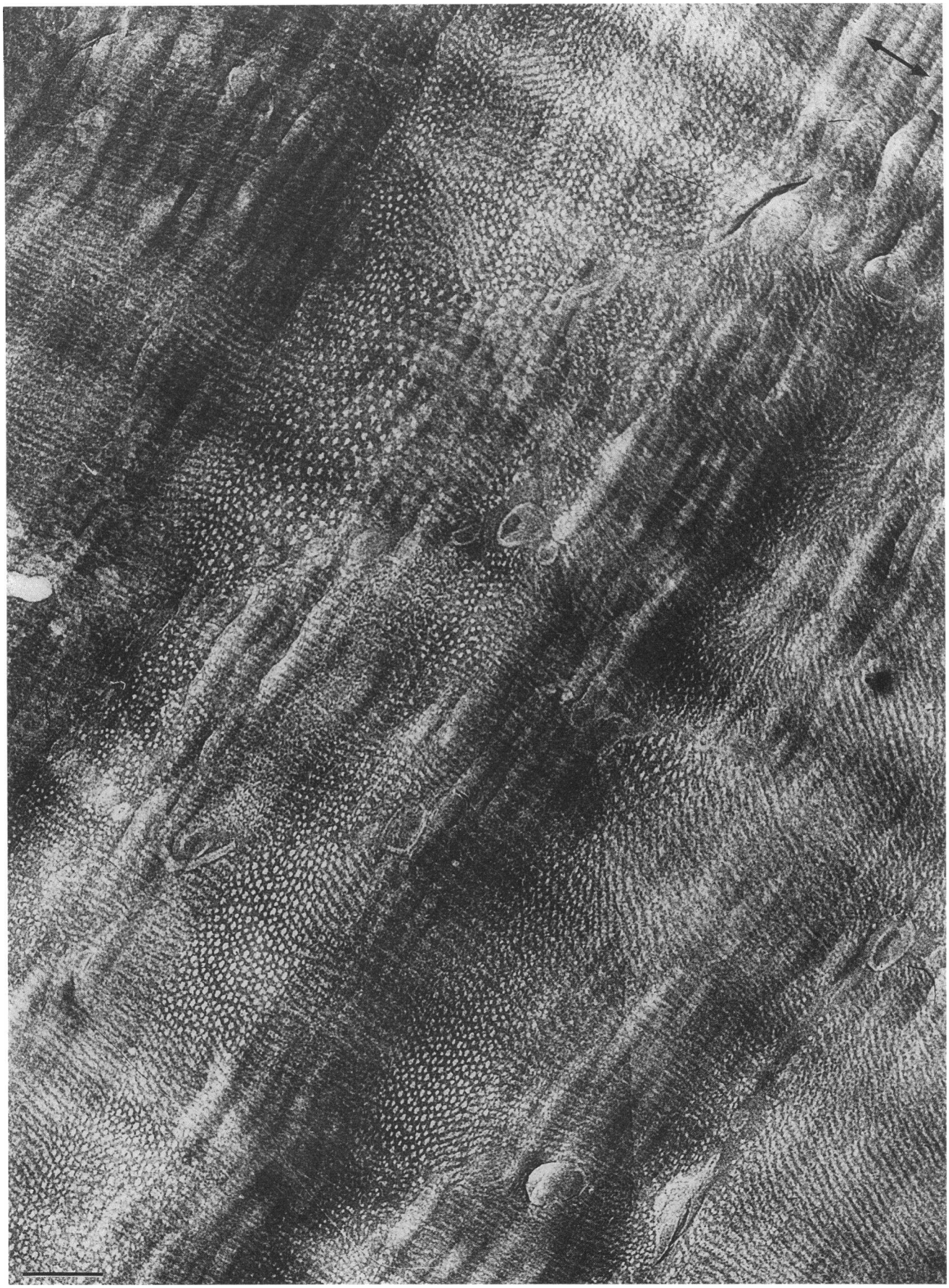

FIGURE 2 Low-magnification field of frozen-hydrated thin section of rabbit psoas muscle fiber in rigor. Its appearance is highly variable over the field, as the result of mechanical distortions. In places, however, small areas of transverse section (hexagonal myofilament lattice) are discernible. The arrow indicates the direction of cutting, i.e., the direction of compression. Perpendicular to it, crumpling and folding of the cryosection is evident in parts of this field. Bar, 0.2 μm.

RESULTS

Freshly excised muscles were prepared in the appropriate physiological states in buffers containing 15% sucrose to suppress the formation of crystalline ice, and frozen rapidly by plunging them into liquid ethane (13). A typical cryosection of rabbit psoas muscle in rigor is shown in Fig. 2. Despite the lack of staining, the section exhibits adequate contrast as a result of the difference in density between the vitreous ice and the embedded protein filaments, accentuated by phase-contrast imaging. However, distortion effects are immediately apparent. For instance, the areas of transverse section are extremely localized in comparison to the expanses seen in conventional sections (e.g., references 6 and 12). Nevertheless, small areas of transverse section may be picked out, and such images from relaxed and rigor specimens are compared in Fig. 3. In both cases, sarcomere segments are shown that contain both myosin and actin filaments (Fig. 3, *a* and *b*), and myosin alone (Fig. 3, *c* and *d*). In all four images, the myofilament lattices depart substantially from hexagonality as the result of compression sustained during sectioning. The compression factor is somewhat variable, but frequently of the order of 50%.

Ultimately, what we wish to determine are quantitative differences between density maps that correspond to the relaxed and rigor states, respectively, and between the dispositions of the myosin filament in the presence and absence of actin. However, several factors preclude drawing such conclusions directly from digitized micrographs of cryosections. First, the projected density of the specimen is not conveyed linearly with this mode of imaging, and the defocus that governs this nonlinearity is somewhat variable from micrograph to micrograph. Second, unit cells vary in appearance over the same myofilament lattice, in consequence of both spatial disordering and a rather low signal-to-noise ratio. Accordingly, image averaging must be performed to make such comparisons statistically meaningful. A sequence of image processing operations designed for this purpose is outlined in Fig. 1, and its efficacy is illustrated in Figs. 4, *b* and *d*, and 6, in terms of diffraction patterns that correspond to the myofilament lattice at successive stages of processing.

The adverse effects of spatial disordering are apparent in the original diffraction pattern (Fig. 4 *b*). The periodic

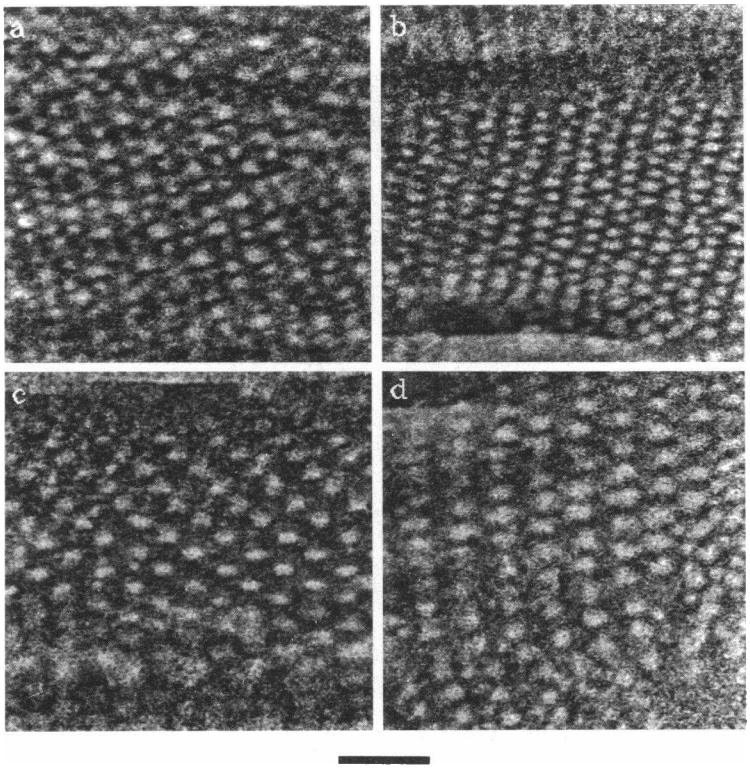

FIGURE 3 Higher-magnification views of areas of transverse thin sections of frozen-hydrated muscle fibers: (*a*) relaxed state, both myosin and actin filaments present; (*b*) rigor state, both myosin and actin filaments present; (*c*) relaxed state, myosin filaments only present; (*d*) rigor state, myosin filaments only present. Bar, 0.2 μm.

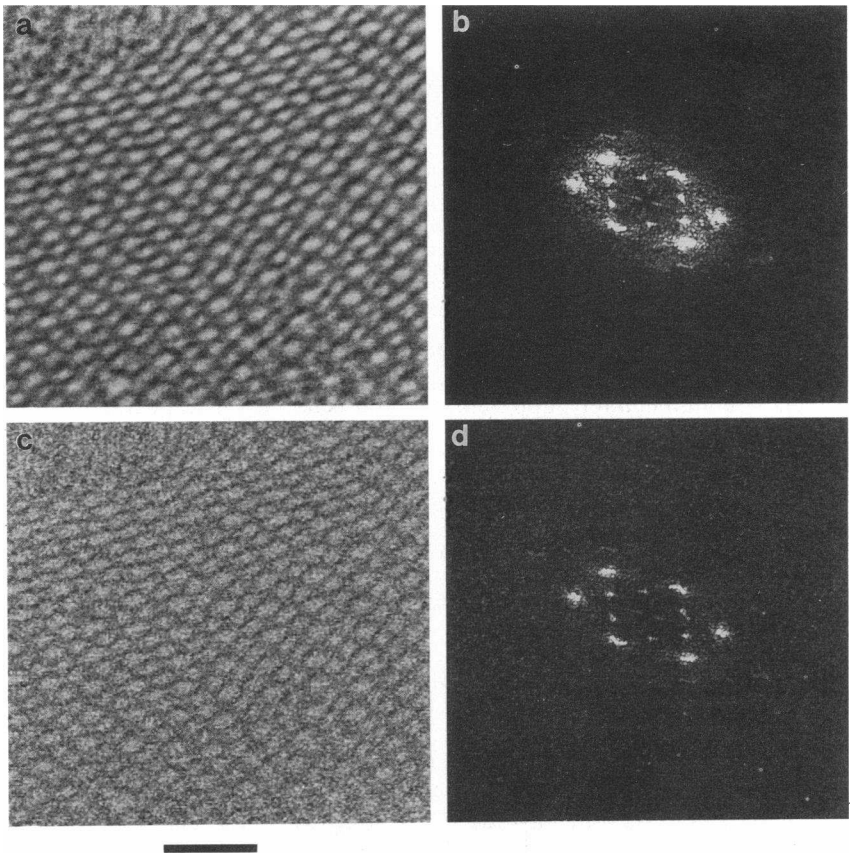

FIGURE 4 A small area of rigor thin section (*a*) was compensated for nouniformity of contrast transfer (restored) as described in Materials and Methods. The same area, after restoration, is shown in *c*. The diffraction patterns of *a* and *c* are shown in *b* and *d*, respectively. Bar, 0.2 μm.

reflections, which index on a quasihexagonal reciprocal lattice are diffuse, and they extend only to the second order. Nonuniformity of contrast transfer resulting from the strongly defocused bright-field imaging is evident from the distribution of background intensity (Fig. 4 *b*). With this particular micrograph, for instance, the second hexagonal order (the *(11)* reflections) is clearly overemphasized relative to the first (the *(10)* reflections). To compensate for this effect, we first constructed a contrast transfer function, then used it for image restoration (Materials and Methods). Fig. 4 *d* shows the uniformity of background intensity thus achieved in the diffraction pattern. The image itself seems to undergo a loss of contrast (really a redistribution of contrast, cf. Fig. 4, *a* and *c*).

To correct for spatial disordering, we have developed a method of correlation averaging based on extracting individual unit cells defined by the centers of four adjacent myosin filaments, and transforming them by interpolation into an array of standard size (Materials and Methods). Finally, each set of unit cells was screened to eliminate anomalous members, whose inclusion would degrade the final averaged image (24). Synthetic arrays of rectified unit cells are shown in Fig. 5 for the relaxed (*a* and *c*) and rigor (*b* and *d*) states, respectively. The unit cells in Fig. 5, *a* and *b*, contains actin filaments, whereas those in *c* and *d* represent the "nonoverlap" region of the sarcomere (i.e., myosin filaments in the absence of actin). The corresponding set of diffraction patterns (amplitude spectra) are presented in Fig. 6. The reciprocal lattices are now hexagonal, and their reflections are much sharper; moreover, they extend to considerably higher spatial frequencies, indicative of the improvement in resolution thus achieved.

The maps of projected density given by the averaged unit cells are compiled in Fig. 7, and the data sets on which these images are based are summarized in Table 2. Where the myosin and the actin filaments overlap, the actin filaments are surprisingly prominent relative to myosin, in comparison with their appearance in conventional thin sections (e.g., references 6 and 12). Indeed, in rigor muscle, it can be rather difficult at first sight to

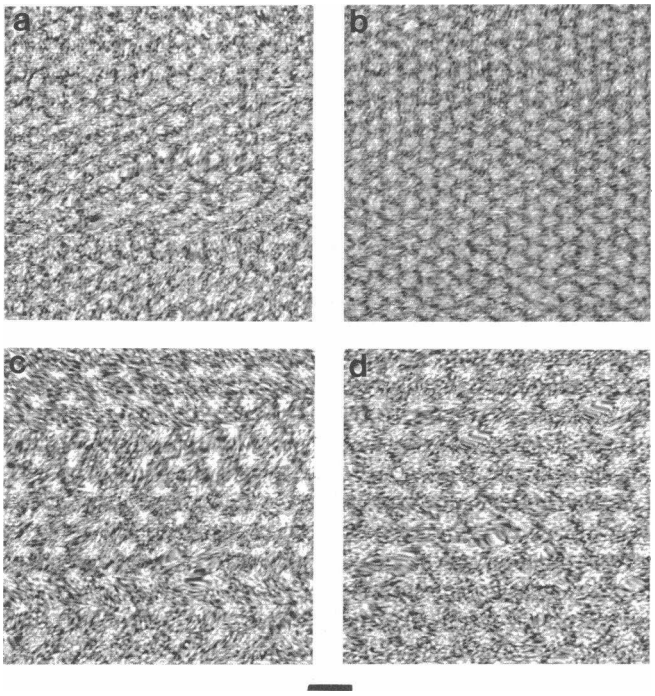

FIGURE 5 Synthetic arrays of myofilament lattice unit cells. Each micrograph contributing to these syntheses was first treated by image restoration, and then corrected for compression and other geometrical distortions by mapping its unit cells on to a cell of standard dimensions. (*a*) Relaxed state, "overlap" region; (*b*) rigor state, "overlap" region; (*c*) relaxed state, "nonoverlap" region; (*d*) rigor state, "nonoverlap" region. Bar, 0.2 μm.

discriminate between the "thick" and the "thin" filaments (e.g., Figs. 3 *b* and 7 *b*). The main difference between the rigor and the relaxed maps is, as expected, a thickening of the actin filaments in rigor, at the expense of the myosin filaments. This effect is illustrated more quantitatively in Fig. 8, in terms of density traces across the respective unit cells (which were normalized so as to contain the same amount of mass). The difference curve (Fig. 8) shows superimposable densities at the core of the actin filament, then a region that gains density in rigor extending to a radius of ~11 nm out from the center of the actin filament and peaking at a radius of ~7 nm. Compensating loss of density takes place in an annular region around the periphery of the myosin filament, extending to a radius of ~12 nm from its center, and peaking at a radius of ~6 nm.

Because the visualized difference between the relaxed myofilament lattice and its rigor state was so slight, we performed a statistical test to confirm its significance. Each unit cell, rigor and relaxed alike, was tested for whether it resembled more closely the average "rigor" unit cell or the average "relaxed" unit cell, with resemblance expressed as proximity in terms of the Euclidean distance[1] between images. If there were to be no significant difference between the rigor and relaxed states (in this representation), approximately half of the "relaxed" unit cells should map closer to the "rigor" average, and vice versa. In fact, >95% of the unit cells mapped closer to the correct reference image, indicating that the distinction between the respective states is sufficiently pronounced to be reproducibly detectable even in the presence of the substantial noise levels encountered in these images.

In the region where there is no overlap with actin, the myosin filaments also look broader in the rigor state (cf. Fig. 7, *c* and *d*). This observation suggests that, even in the absence of actin filaments, the myosin molecules undergo a conformational change upon entering the rigor state, whereby the cross-bridges move further out from the filament backbone.

DISCUSSION

Resolution of electron density maps of the myofilament lattice

The main thrust of this study has been to devise and apply methods for analyzing electron micrographs of frozen-hydrated thin sections of muscle tissue, to extract information on the myofilament lattice in its native state. Our procedure first corrects the images for nonuniformity of contrast transfer, and then compensates for spatial disordering caused by cutting-induced compression and other sources of distortion. Finally, the initially high noise level is suppressed by averaging over many unit cells.

A major source of spatial disordering is cutting-induced compression which, consistent with earlier work (13), we found to be on a substantial scale, with compression factors of 0.5–0.7 common. With a view to *a posteriori* correction for compression, muscle is a particularly tractable specimen in the sense that its hexagonal lattice serves as a local built-in compression meter, and similar methods could be applied to other regular specimens. However, inferences based on cryosections concerning the dimensions of nonperiodic specimens are likely to be more problematic.

The improvement in resolution achieved in our analysis is illustrated in the diffraction patterns of synthetic arrays of unit cells, where the (31) reflection at $(11\ \text{nm})^{-1}$ is visible above background in both the "relaxed" and the "rigor" patterns (Fig. 6, *a* and *b*). In comparison, the

[1](Euclidean distance)^2 = sum of squares of the differences between corresponding pixels in the images under comparison.

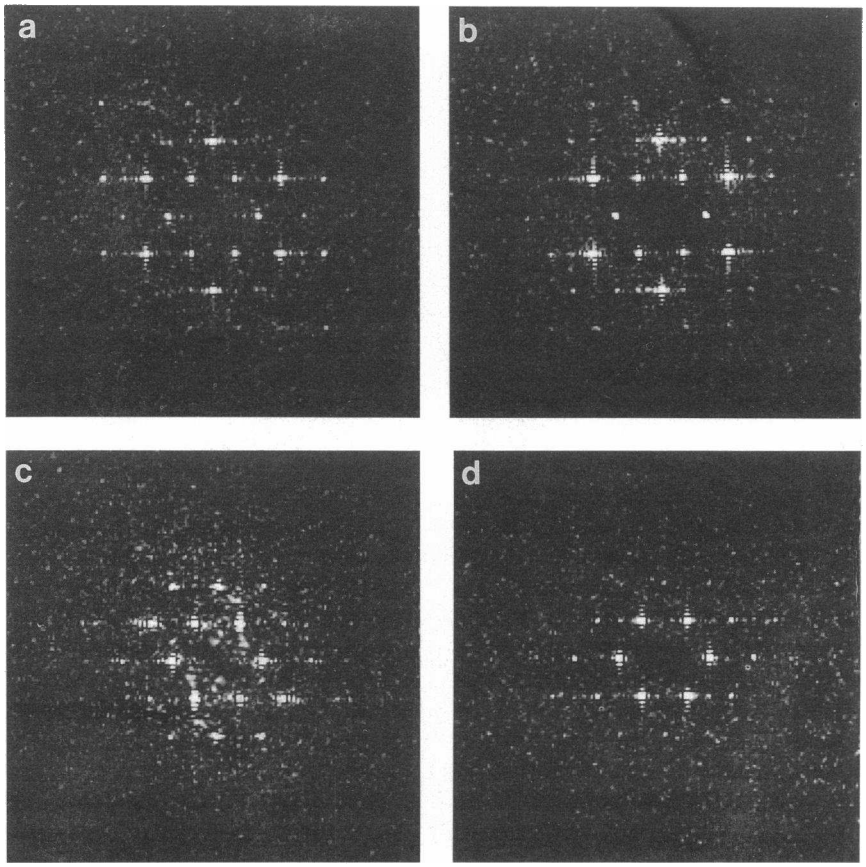

FIGURE 6 Diffraction patterns (amplitude spectra) of the myofilament lattice images shown in Fig. 5.

diffractograms of the original micrographs extend only to the *(11)* reflection at (23 nm)$^{-1}$ (Fig. 4 *b*). The SSNR measure of resolution (26) provides a more objective and quantitative generalization of the method of counting diffraction orders. It gives figures that range from 10.1 nm resolution for the "rigor, overlap" density map, to 15.6 nm for the "rigor, nonoverlap" map.

Density maps as probability distributions

One factor underlying the relatively modest nominal resolution of our density maps is the existence of real (intrinsic) variability (as opposed to random additive noise) among the individual unit cell projections. We estimate these sections to be 100–150 nm thick, so that each unit cell contains 20–30 myosin molecules. This number is sufficiently small that, in view of the conformational alternatives open to myosin "heads", even in the same physiological state, the projections of different unit cells in a transverse section would be expected to vary significantly, even in the absence of noise. This intrinsic variability is illustrated in "standard deviation" maps (not shown) or density fluctuations from unit cell to unit cell. These fluctuations are nonuniform over the unit cell area, and are most pronounced in the interfilament spaces, presumably reflecting variability in the net configurations of the unit cells' complements of S1-cross-bridges.

The SSNR resolution criterion (reference 26, cf. above) is based on a measure of mutual consistency between all elements compared, and thus does not distinguish between genuine variability of the kind noted above, and random additive noise. Accordingly, SSNR-defined resolution will appear lower for the myofilament lattice than for a genuine crystal analyzed in the same way. In this respect, the map of projected density given by the final average relates to a probability distribution, and not a universal signal from which each unit cell differs only by random noise.

Comparison with x-ray results

It has long been known that the transition from relaxation to rigor, as monitored by x-ray fiber diffraction, is expressed as a change in the relative intensities of the *(10)*

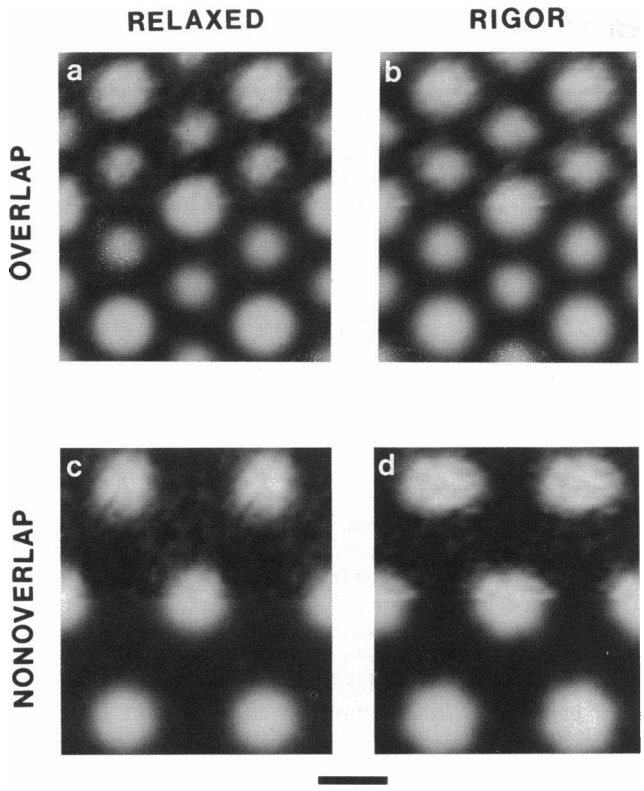

FIGURE 7 Myofilament lattice maps of density projected in the axial direction, obtained by averaging individual unit cells from frozen-hydrated thin sections. The data were first preprocessed to the stage represented by Fig. 5, and then averaged. (*a*) Relaxed state, "overlap" region; (*b*) rigor state, "overlap" region; (*c*) relaxed state, "nonoverlap" region; (*d*) rigor state, "nonoverlap" region. In the bottom half of each panel, sixfold symmetry has been imposed. Bar, 0.2 μm. In *d*, the projected myosin filament appears slightly elliptical in cross-section as a result of residual tilt, i.e., the contributing sections not being exactly transverse. However, the scan across its minor axis (not shown) reveals a filament that is still appreciably wider than in the relaxed state.

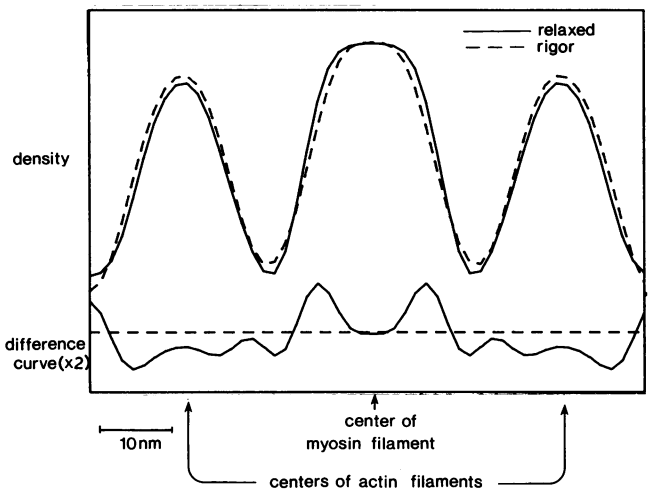

FIGURE 8 Transverse traces of projected density taken across the unit cell maps of projected density for the rigor and relaxed states of rabbit psoas muscle, as calculated from electron micrographs of frozen-hydrated thin sections.

and the *(11)* equatorial reflections (reference 6). The corresponding measurement in our analysis involves consulting the appropriate terms of the Fourier transforms of the respective density maps. These data are compiled in Table 3, together with the phase information for the reflections solved so far. The ratio between the two lowest order amplitudes, viz. F_{11}/F_{10} (rigor) is 2.7, which is very close to the value of 2.9 obtained in a recent x-ray diffraction study of rabbit psoas muscle (10) under the same conditions, other than the absence of cryoprotectant. For the relaxed state, the corresponding ratios are 2.0 (cryo-EM) and 1.4 (x-ray, reference 10). Overall, we consider that the agreement between these two entirely different techniques is remarkably good, and attests to the efficacy of our empirical method of image restoration. There are, however, certain factors that may be expected to preclude perfect agreement: (*a*) The structure factors for the scattering of electrons and x-rays respectively from solvent and protein are different. (*b*) Because the x-ray diffraction experiments (10) were performed at the sarcomere lengths of 2.2–2.4 μm where the myosin filaments overlap for almost all their length with actin filaments, this comparison was based on Fourier amplitudes calculated from the "overlap" density maps (Fig, 7 *a* and *b*, Table 3). Nevertheless, although the x-ray equatorial reflections are dominated by scattering from the overlap region (5), other parts of the sarcomere do

TABLE 2 Statistics and resolution achieved in cryoelectron microscopic analysis of the myofilament lattice in two states (relaxed and rigor) and for two regions of the sarcomere (overlap and nonoverlap)

	Relaxed/overlap	Rigor/overlap	Relaxed/nonoverlap	Rigor/nonoverlap
No. of unit cells analyzed	204	180	131	124
No. of unit cells approved	129	104	105	116
Resolution (*nm*)*	10.1	10.7	14.6	15.7

*The resolution was calculated according to the SSNR criterion (23), viz, the highest spatial frequency to which the SNR maintained a value >4.

TABLE 3 Phases and amplitudes for reciprocal myofilament lattice reflections from the Fourier transforms of unit cell maps of projected density

	Relaxed state				Rigor state			
	Method A		Method B		Method A		Method B	
Reflection	Amplitude*	Phase‡	Amplitude*	Phase‡	Amplitude*	Phase‡	Amplitude*	Phase‡
		Degrees		*Degrees*		*Degrees*		*Degrees*
(1,0)	1,000	0	1,009	0 ± 2.8	861	0	916	0 ± 17
(1,1)	1,988	0	1,998	0 ± 2.5	2,306	0	2,320	0 ± 3.7
(2,0)	14	(180)	176	180 ± 109	101	180	237	180 ± 71
(2,1)	181	180	266	180 ± 53	221	180	247	180 ± 25
(1,2)	305	180	351	180 ± 7	206	180	222	180 ± 17
(3,0)	10	(180)	152	180 ± 116	86	(180)	218	180 ± 96
(2,2)	165	180	186	180 ± 7	132	180	143	180 ± 18
(3,1)	107	180	175	180 ± 32	11	(180)	65	180 ± 107
(1,3)	125	180	143	180 ± 22	8	0	125	0 ± 107

These sets of amplitudes and phases were derived from the digital Fourier transforms of averaged myofilament lattice unit cells ("overlap" maps, cf., Fig. 7, *a* and *b*). In method A, the unit cells were sixfold symmetrized, so that the phases are all 0 or 180°. A reflection, (h, k), for which there was, before symmetrization, little consistency between the three Fourier orders related to it, has a low amplitude and an indeterminate phase (parentheses). With method B, no symmetrization was imposed, and the amplitude given is the root-mean-square of three contributing Fourier terms. The criteria for a well-determined reflection with a favorable signal-to-noise ratio are that the amplitudes given by the two methods should be close in value, and that the phase uncertainty given by method B should be low. *The normalization of the unit cells (and consequently of their Fourier transforms) is described in the last section of Materials and Methods, and scaled according to an assignment of the value 1,000 to the $F_{1,0}$ (relaxed) amplitude. ‡The uncertainty assigned to each phase is the amplitude-weighted root-mean-square over these three symmetry-related terms. In the event of pure noise, these terms would be uncorrelated arbitrary phasors and would therefore result in an expected phase uncertainty of 104° in this convention. Accordingly, an uncertainty of 60° or less corresponds to a phase determination that inspires a reasonable degree of confidence.

contribute to the pattern, and could thus affect this comparison. (*c*) The amplitudes obtained in an x-ray diffraction study depend, to some extent, on the specific procedure used to "strip" the background scattering curve from the discrete reciprocal lattice reflections. Consistent use of the same procedure allows highly reproducible determinations of amplitudes (8). However, when these data are compared with amplitudes from some other source (such as cryo-EM), the choice of stripping procedure is a source of ambiguity. The associated margin of uncertainty is likely to be fairly small for the *(10)* and *(11)* reflections, but increasingly important for higher orders.

Effects of sucrose as cryopreservative

Another possible source of inconsistency between the x-ray and cryo-EM data concerns the use of sucrose as a cryoprotectant. A 15% concentration of sucrose, although close to the minimum amount required to suppress the formation of destructive hexagonal-phase ice crystals, may be high enough to cause structural alteration of the myofilament matrix. To address this question, preliminary x-ray diffraction experiments have been performed on sucrose-perfused muscle fibers (Podolsky, R. J., M.-L. Barbosa, and L. C. Yu, unpublished observations). The results show not only the expected diminution of contrast (weakening of reflections), but also suggest a change in the relative intensities of *(10)* and *(11)*, particularly for the relaxed state. Thus it may be that the myofilament lattice structure is altered somewhat by the presence of sucrose. Muscle perfused with sucrose is, however, functional in the sense of being capable of generating force. ~90% of the full isometric force is developed by skinned rabbit muscle fibers perfused with 15% sucrose, upon activation by calcium (Horowits, R., personal communication).

Visualization of the relaxed → rigor transition

We conclude from this analysis that the structural changes undergone in the transition from relaxed to rigor state, as perceived in axial projection (Figs. 7 and 8), amount to an egress of density from an annular zone surrounding the myosin filament backbone and a compensating accumulation of density around the actin filaments. It is striking that, in rigor, the "thin filament" is almost as thick as the "thick filament", and presumably conveys, in projection, the net binding configuration of all or almost all cross-bridges to actin filaments (29–31). The fact that the "relaxed" projection is not greatly different suggests that, in relaxed muscle at 100 mM ionic strength, the cross-bridges are not confined to the immediate proximity of the myosin backbone. However, we cannot yet say whether significant numbers of them are

actually in contact with actin filaments, as has been suggested on the basis of mechanical stiffness measurements (32).

Rigor-induced change of the myosin filament in the absence of actin

It is of interest that, on entering rigor, myosin filaments in the H-zone (i.e., the part of the A-band where they do not overlap with actin filaments) appear to broaden. Thus the immediate proximity of actin filaments may not be necessary for cross-bridges to move away from the myosin filament backbone. Other observations that have also suggested such an effect are (*a*) the disappearance of "myosin" layer lines from the x-ray diffraction pattern of frog muscle fibers when subjected to rigor-inducing treatments after being stretched to nonoverlap lengths (33), and (*b*) the reversible disruption, upon ATP deprivation, of the regular cross-bridge arrangement on thick myosin filaments initially isolated from insect flight muscle in the presence of ATP, as visualized by negative-staining electron microscopy (34).

Concluding remarks

The present results demonstrate that quantitative measurements of the distribution of mass within native myofilament lattices are possible by combining appropriate image analysis with low-dose electron microscopy of thin sections of muscle fibers preserved in vitreous ice. In this initial study, we have characterized the relaxed and rigor states of rabbit psoas muscle at 100 mM ionic strength. Now that the basic methodology has been worked out, it will be of interest to apply it to other physiological states, such as relaxed muscle at lower ionic strength (20 mM) where large numbers of weakly bound cross-bridges are thought to be formed (10, 35), and in particular to muscle activated at physiological ionic strength (170–200 mM) where normal force-generating cross-bridges are formed. In the longer term (and anticipating some progress towards solving the remaining technical limitations), it may become possible to investigate the dynamic development of force generation in studies whereby successive time-points of the activation process are sampled by rapid and temporally specific freezing.

We thank Dr. Daniel Thomas for a valuable suggestion at the outset, Dr. Leepo Yu for useful advice and making available unpublished data, Dr. Maria Barbosa for stimulating and helpful input to this project, and Ms. Margaret Bisher for help with photography.

Received for publication 9 August 1988 and in final form 28 November 1988.

REFERENCES

1. Huxley, A. F., and R. Niedergerke. 1954. Interference microscopy of living muscle fibers. *Nature (Lond.)*. 173:971–973.
2. Huxley, H. E., and J. Hanson. 1954. Changes in the cross-striations of muscle during contraction and stretch and their structural interpretation. *Nature (Lond.)*. 173:973–976.
3. Squire, J. M. 1981. The Structural basis of Muscular Contraction. Plenum Publishing Corp., New York. 8–16, 524–527.
4. Pollard, T. D. 1987. The myosin crossbridge problem. *Cell*. 48:909–910.
5. Elliott, G. F., J. Lowy, and C. K. Worthington. 1963. An x-ray and light diffraction study of the filament lattice of striated muscle in the living state and in rigor. *J. Mol. Biol.* 6:295–305.
6. Huxley, H. E. 1968. Structural difference between resting and rigor muscle: evidence from intensity changes in the low-angle equatorial x-ray diagram. *J. Mol. Biol.* 37:507–520.
7. Haselgrove, J. C., and H. E. Huxley. 1973. X-Ray evidence for radial cross-bridge movement and for the sliding filament model in actively contracting muscle. *J. Mol. Biol.* 77:549–568.
8. Yu, L. C., A. C. Steven, G. R. S. Naylor, R. C. Gamble, and R. J. Podolsky. 1985. Distribution of mass in relaxed frog skeletal muscle and its redistribution upon activation. *Biophys. J.* 47:311–321.
9. Harford, J., and J. Squire. 1986. "Crystalline" myosin cross-bridge array in relaxed bony fish muscle. *Biophys. J.* 50:145–155.
10. Brenner, B., L. C. Yu, and R. J. Podolsky. 1984. X-Ray diffraction evidence for cross-bridge formation in relaxed muscle fibers at various ionic strengths. *Biophys. J.* 46:299–306.
11. Reedy, M. K. 1968. Ultrastructure of insect flight muscle. I. Screw sense and structural grouping in the rigor cross-bridge lattice. *J. Mol. Biol.* 31:155–176.
12. Luther, P. K., P. M. G. Munro, and J. M. Squire. 1981. Three-dimensional structure of the vertebrate muscle A-band. III. M-Region structure and myosin filament symmetry. *J. Mol. Biol.* 151:703–730.
13. McDowall, A. W., W. Hofmann, J. Lepault, M. Adrian, and J. Dubochet. 1984. Cryo-electron microscopy of vitrified insect flight muscle. *J. Mol. Biol.* 178:105–111.
14. Dubochet, J., and A. W. McDowall. 1984. Frozen hydrated sections. *In* Science of Biological Specimen Preparation. J.-P. Revel, T. Barnard, and G. H. Haggis, editors. Scanning Electron Microscopy Inc., Chicago. 147–152.
15. Stewart, M., and G. Vigers. 1986. Electron microscopy of frozen-hydrated biological material. *Nature (Lond.)*. 319:631–636.
16. Dubochet, J., M. Adrian, J.-J. Chang, J.-C. Homo, J. Lepault, A. McDowall, and P. Schultz. 1988. Cryo-electron miscroscopy of vitrified specimens. *Q. Rev. Biophys.* 21:129–228.
17. McGee, P. A., B. L. Trus, and A. C. Steven. 1982. Techniques to evaluate the performance of scanning microdensitometers in the digitization of electron micrographs. *Micron*. 13:221–228.
18. Trus, B. L., and A. C. Steven. 1981. Digital image processing of electron micrographs—the PIC system. *Ultramicrosopy*. 6:383–386.
19. Misell, D. L. 1978. Image Analysis, Enhancement and Interpretation. North-Holland Publishing Co., Amsterdam. 59–66 and 169–171.
20. Steven, A. C., P. R. Smith, and R. W. Horne. 1978. Capsid fine structure of cowpea chlorotic mottle virus: from a computer

analysis of negatively stained virus arrays. *J. Ultrastruc. Res.* 64:63–73.

21. Henderson, R., and P. N. T. Unwin. 1975. Three-dimensional model of purple membrane obtained by electron microscopy. *Nature (Lond.).* 257:28–32.
22. Frank, J. 1980. The role of correlation techniques in computer image processing. *In* Computer Processing of Electron Microscopic Images. P. W. Hawkes, editor. Springer-Verlag, Berlin. 187–222.
23. Crowther, R. A., and U. B. Sleytr. 1977. An analysis of the fine structure of the surface layers of two strains of *Clostridia,* including correction for distorted images. *J. Ultrastruc. Res.* 58:41–49.
24. Smith, P. R., and U. Aebi. 1976. The computer filtration of hexagonal lattices. *J. Supramol. Struct.* 5:493–495.
25. Unser, M., A. C. Steven, and B. L. Trus. 1986. Odd men out: a quantitative objective procedure for identifying anomalous members of a set of noisy images of ostensibly identical specimens. *Ultramicroscopy.* 19:337–348.
26. Unser, M., B. L. Trus, and A. C. Steven. 1987. A new resolution criterion based on spectral signal-to-noise ratios. *Ultramicroscopy.* 23:39–52.
27. Lee, B. 1983. Calculation of volume fluctuation for globular protein models. *Proc. Natl. Acad. Sci. USA.* 80:622–626.
28. Gavish, B., E. Gratton, and C. J. Hardy. 1983. Adiabatic compressibility of globular proteins. *Proc. Natl. Acad. Sci. USA.* 80:750–754.
29. Lovell, S. J., and W. F. Harrington. 1981. Measurement of the fraction of myosin heads bound to actin in rabbit skeletal myofibrils in rigor. *J. Mol. Biol.* 149:659–674.
30. Cooke, R., and K. Franks. 1980. All myosin heads form bonds with actin in rigor rabbit skeletal muscle. *Biochemistry.* 19:2265–2269.
31. Cooke, R., and D. Thomas. 1980. Spin-label studies of the structure and dynamics of glycerinated muscle fibers. Saturation transfer EPR studies on rigor labeled fibers. *Fed. Proc.* 39:1962.
32. Schoenberg, M. 1988. Characterization of the myosin adenosine triphosphate (M.ATP) cross-bridge in rabbit and frog skeletal muscle fibers. *Biophys. J.* 54:135–143.
33. Haselgrove, J. C. 1975. X-Ray evidence for conformational changes in the myosin filaments of vertebrate striated muscle. *J. Mol. Biol.* 92:113–143.
34. Clarke, M. L., W. Hofmann, and J. S. Wray. 1986. ATP binding and crossbridge structure in muscle. *J. Mol. Biol.* 191:581–585.
35. Brenner, B., M. Schoenberg, J. M. Chalovich, L. E. Greene, and E. Eisenberg. 1982. Evidence for cross-bridge attachment in relaxed muscle at low ionic strength. *Proc. Natl. Acad. Sci. USA.* 79:7288–7291.